catalysts

MDPI

Article

Understanding the Heteroatom Effect on the Ullmann Copper-Catalyzed Cross-Coupling of *X*-Arylation (*X* = NH, O, S) Mechanism

Diego M. Andrada [1,2,*], Silvia M. Soria-Castro [3], Daniel A. Caminos [3], Juan E. Argüello [3] and Alicia B. Peñéñory [3]

1 Krupp-Chair of General and Inorganic Chemistry, University of Saarland, Campus C4.1, 66123 Saarbruecken, Germany
2 Fachbereich Chemie, University of Marburg, Hans-Meerweinstrasse 4, 35032 Marburg, Germany
3 INFIQC, Departamento de Química Orgánica, Facultad de Ciencias Químicas, University of Córdoba, Ciudad Universitaria, Córdoba X5000HUA, Argentina; ssoriacastro@fcq.unc.edu.ar (S.M.S.-C.); dcaminos@fcq.unc.edu.ar (D.A.C.); jea@fcq.unc.edu.ar (J.E.A.); penenory@fcq.unc.edu.ar (A.B.P.)
* Correspondence: diego.andrada@uni-saarland.de; Tel.: +49-681-302-71669

Received: 14 November 2017; Accepted: 11 December 2017; Published: 13 December 2017

Abstract: Density Functional Theory (DFT) calculations have been carried out in order to unravel the governing reaction mechanism in copper-catalyzed cross-coupling Ullmann type reactions between iodobenzene (**1**, PhI) and aniline (**2-NH**, $PhNH_2$), phenol (**2-O**, PhOH) and thiophenol (**2-S**, PhSH) with phenanthroline (phen) as the ancillary ligand. Four different pathways for the mechanism were considered namely Oxidative Addition–Reductive Elimination (OA-RE), σ-bond Metathesis (MET), Single Electron Transfer (SET), and Halogen Atom Transfer (HAT). Our results suggest that the OA-RE route, involving Cu^{III} intermediates, is the energetically most favorable pathway for all the systems considered. Interestingly, the rate-determining step is the oxidative addition of the phenyl iodide to the metal center regardless of the nature of the heteroatom. The computed energy barriers in OA increase in the order O < S < NH. Using the Activation Strain Model (ASM) of chemical reactivity, it was found that the strain energy associated with the bending of the copper(I) complex controls the observed reactivity.

Keywords: copper-catalyst; Ullmann; cross-coupling; Density Functional Theory (DFT); activation strain model

1. Introduction

Nowadays, copper-catalyzed cross-coupling Ullmann type reactions are considered among the most useful processes in the synthesis to build C–C, C–N, C–O, C–S, C–P, and C–Se bonds [1–6]. Despite its undoubtedly current success, after the seminal work by Fritz Ullmann [7–9] and Iram Goldberg [10] in the early 20th century, these reactions did not garner considerable attention from the synthetic community. This was a consequence of the harsh reaction condition requirements such as stoichiometric amounts of copper, strong bases, high temperatures, and long reaction times [11]. These drawbacks were overcome at the beginning of the new century with the introduction of the ancillary chelating ligands (L) approach by the groups of Taillefer [12] and Buchwald [13] representing thus a major breakthrough in copper chemistry. The use of bidentate ligands like phenanthroline [14–18], diamines [19–21], amino acids [22–24], and 1,3-diketones [25,26] among others [27–30] has not only met the demands of reliability, mildness, and functional group tolerance but also interesting modern features such as orthogonal reactivity [26]. The applications so far known

have been spread over a diverse range of areas from pharmaceutical [31] and natural products [32–34] to materials fields [35,36].

The mechanistic details of how the carbon-heteroatom C–X (*X* = N, O, and S) bonds are formed have remained for a long time somewhat unclear [4]. Since the rate-limiting step is usually at the initial stages of the reaction, the detection of intermediate species has been very rare. Thus, most of the mechanistic proposals which shed light on this area are drawn from kinetic experimental and computational studies [37,38]. While most of the evidence collected so far has shown that the active catalyst is a ligand-copper(I)-nucleophile [(L)Cu^{I}(Nu)] species, there is no such agreement on the way this catalyst activates the aryl halide (ArY, Y = Cl, Br and I). The most invoked routes are based on either one-electron redox processes through the radical intermediate Cu^{I}/Cu^{II} catalytic cycle namely Single Electron Transfer (SET) and Halogen Atom Transfer (HAT) [4,39–42], or on two-electron redox processes via a Cu^{I}/Cu^{III} catalytic cycle like Oxidative Addition–Reductive Elimination (OA-RE) or σ-bond Metathesis (MET) (Scheme 1) [37,38,43–50].

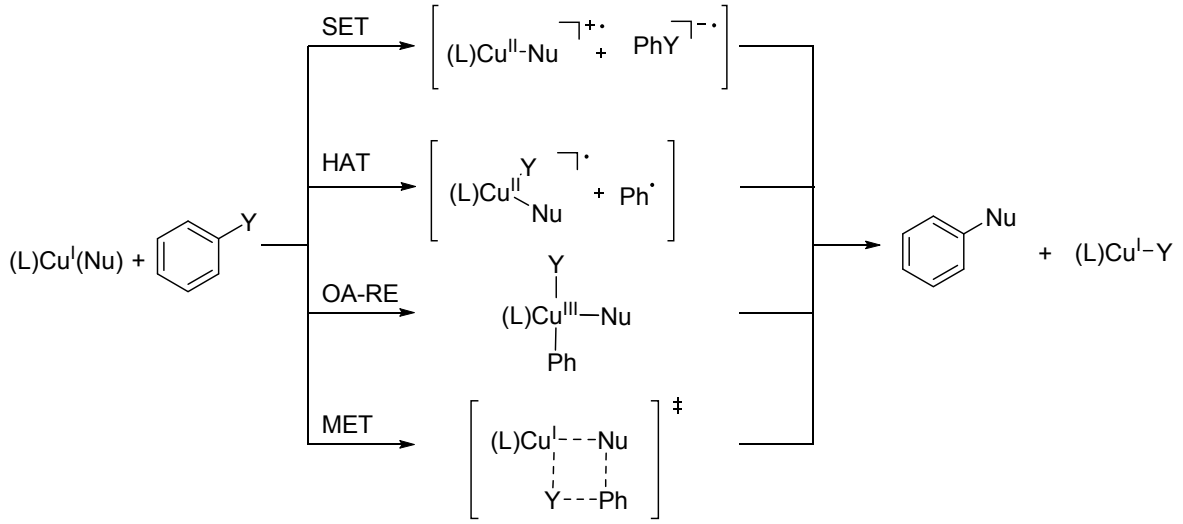

Scheme 1. The four most invoked reaction mechanisms of Ullman-type reactions. Single Electron Transfer (SET), Halogen Atom Transfer (HAT), Oxidative Addition–Reductive Elimination (OA-RE) and σ-bond Metathesis (MET) [51].

In the last twenty years, a particular effort has been addressed to elucidate the mechanistic details concerning the catalytic copper-catalyzed *N*-, *O*-, and *S*-arylations. Thus, Buchwald et al. started a program to kinetically investigate the *N*-arylation of amides and alkylamines [20,21,52,53] and *O*-arylation of aliphatic alcohols [26,54,55]. They clearly showed that the aryl halide activation occurs by the [(L)Cu^{I}(Nu)] complexes. In this regard, Hartwig et al. were able to isolate and characterize a number of copper imidate, amidate, amino, phenoxide, and thiophenoxide complexes which are chemically competent to couple a variety of aryl halides [40,42,56]. The studies carried out on the reactivity of these complexes, including kinetic studies and radical clock experiments, argued against pathways involving radical intermediates. Conversely, Buchwald and Houk by experimental and computational methods claimed that the SET and HAT mechanisms are energetically more favorable for Ullmann *N*- and *O*-arylation of alkyl amines and alcohols with aryl iodides [51]. Further support to these one-electron mechanisms was given by a number of detailed theoretical studies on the *N*-, *O*-, and *S*-arylation reported by Zhang and co-workers [57–61]. They confirmed that [(L)Cu^{I}(Nu)] species is indeed the most reactive towards aryl halide among all the other possible copper species. Additionally, they concluded that *N*-arylation reactions should occur via an OA-RE mechanism while for the *O*- and *S*-arylation reaction HAT is the most likely pathway. In this context, we recently reported the use of Ullmann reactions under conventional and microwave conditions as a simple and economical process to accomplish a variety of thioacetates and sulfur heterocycles [62]. Lately, we have also contributed to the understanding of this *S*-arylation reaction mechanism by a

combination of experimental and computational studies [63]. Remarkably, no evidence of the presence of radical species was found during the reaction process.

In this sense, very little is known about the factors leading to the observed mechanisms and their influence on reactivity. In line with our ongoing interest in the underlying mechanisms on Ullmann-type reactions, we present herein a detailed Density Functional Theory (DFT) computational study on the copper-catalyzed cross-coupling reaction between phenyl iodine and aniline, phenol and thiophenol as the nucleophile in the presence of 1,10-phenanthroline (phen) as a ligand (Scheme 2). In an effort to understand the mechanism of these transformations, we examined the energy profile of different reaction pathways. A deeper understanding of the origins of the reaction barriers was obtained by means of the so-called activation strain model (ASM).

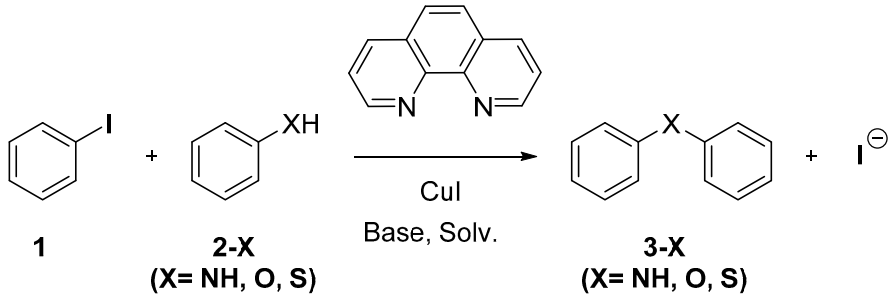

Scheme 2. Copper-catalyzed cross-coupling Ullmann type reaction studies. Base (Cs_2CO_3 and KO^tBu) and solvent (toluene and acetonitrile).

2. Results and Discussion

We first considered the thermodynamics of the formation of the active species [(phen)Cu^I(NHPh)], [(phen)Cu^I(OPh)], and [(phen)Cu^I(SPh)] and their disproportion (Scheme 3). As it was reported elsewhere [57,60,64], there are many copper species that can be formed depending on the reaction conditions. The disproportionation process usually leads to inactive species. Table 1 collates the thermodynamic data for the formation in the gas phase (gas), toluene (tol), and acetonitrile (acn) in the presence of Cs_2CO_3 and KO^tBu as bases. The Gibbs energies computed for the formation of the complexes [(phen)Cu^I(XPh)] follow the trend according to the pK_a of the nucleophiles, i.e., pK_a($PhNH_2$) = 27.0, pK_a(PhOH) = 9.95, and pK_a(PhSH) = 6.5. In concordance with the experiments outcomes [60,65], the formation of the [(phen)Cu^I(SPh)] complex is favored in all the conditions here computed, while the formation of [(phen)Cu^I(NHPh)] and [(phen)Cu^I(OPh)] requires stronger bases. After their formation, these complexes can further disproportionate to generate the ionic species $[Cu^I(phen)_2]^+$ and $[Cu^I(XPh)_2]^-$. This phenomenon has been experimentally and computationally observed by Fiaschi et al. [66,67], Chen et al. [42], and Zhang et al. [59–61]. Our results show that this disproportionation is unfavorable in nonpolar solvents while it becomes favored when the dipolar constant of the solvent increases, in good agreement with previously reported results [59–61].

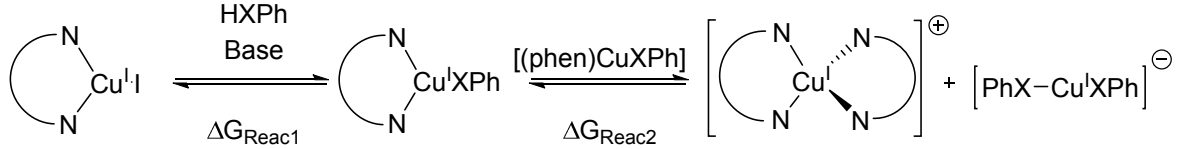

Scheme 3. Equilibrium between the possible copper species (*X* = NH, O, and S).

Table 1. Gibbs Free Energies (kcal/mol) for active copper [(phen)Cu^{I}(XPh)] (*X* = NH, O, and S) complex formation (Reaction 1) and disproportionation (Reaction 2) in different solvents.[1]

Reaction	PhNH$_2$			PhOH			PhSH		
	ΔG_{gas}	ΔG_{tol}	ΔG_{acn}	ΔG_{gas}	ΔG_{tol}	ΔG_{acn}	ΔG_{gas}	ΔG_{tol}	ΔG_{acn}
1 (Cs_2CO_3)	15.2	8.2	2.3	8.5	0.6	−5.8	−4.2	−12.4	−19.4
1 (KO^{t}Bu)	0.2	−3.2	−7.7	−6.5	−10.8	−15.8	−19.2	−23.8	−29.4
2	44.7	13.7	−3.4	40.4	10.6	−6.0	46.9	16.4	−0.7

[1] All calculations were computed at the PCM-[B3LYP + D3(BJ)/def2-TZVPP//B3LYP/def2-SVP] level of theory.

Figure 1 displays the geometry of the [(phen)Cu^{I}(XPh)] complexes together with their dissociation energies. In all complexes, the copper is planar three-coordinated. Interestingly, the 1,10-phenanthroline ligand is not symmetrically bound to the metal center. The Cu^{I}–N(phen) bond distance differences are bigger for the amido complex (0.322 Å) and smaller for the thiophenoxide complex (0.086 Å). Such a distortion from the trigonal geometry of the d^{10} metal center as T-shaped has been observed in other complexes [68]. This is a consequence of the strong σ- and π-donor character of the ligands which leads to the electron-rich copper(I) center, leaving the second nitrogen less coordinated. On the other hand, the Cu–X bond distances are predicted to be 1.860 Å (*X* = N), 1.845 Å (*X* = O), and 2.185 Å (*X* = S). The Cu–NHPh bond distance is within the range of distances reported for the Cu^{I}-amido complexes (~1.865 Å). As expected, the Cu–O and Cu–S bond distances are shorter than those found for the dimer, i.e., 2.066 Å [66] and 2.340 Å [42] for Cu–O and Cu–S bonds, respectively. Additionally, the Cu–S distance is also slightly longer than those measured by Kaim and co-worked for thiolate copper complexes (ca. 2.145 Å) [68]. The computed Cu–X bond dissociation energies clearly indicate that stability of the complexes decreases in the sense NH > S > O.

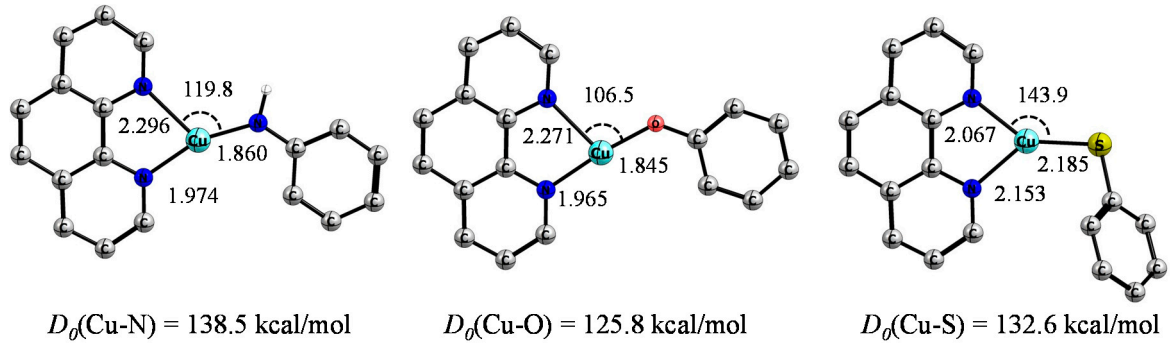

Figure 1. Optimized structures (B3LYP/def2-SVP) and bond dissociation energies D_0(Cu-X) (B3LYP + D3(BJ)/def2-TZVPP//B3LYP/def2-SVP) for the complexes [(phen)Cu^{I}(NHPh)], [(phen)Cu^{I}(OPh)], and [(phen)Cu^{I}(SPh)]. Bond lengths and angles are in [Å] and [°], respectively. The hydrogen atoms attached to carbon atoms are omitted for clarity.

We next calculated the energy of the key steps for the most probable pathways for the formation of cross-coupling products PhXPh (**3-X**, *X* = NH, O, and S) starting with the complexes [(phen)Cu^{I}(NHPh)], [(phen)Cu^{I}(OPh)], and [(phen)Cu^{I}(SPh)]. We considered only the four most appealed mechanisms displayed in Scheme 1. Figure 2 displays the computed Gibbs energy profiles for the *N*-, *O*-, and *S*-arylation of PhI in the gas phase. Additionally, Table 2 summarizes the effects of the solvent in these energy profiles.

The single electron transfer from the [(phen)Cu^{I}(XPh)] complex to PhI forming the radical cation Cu^{II} intermediate complex, phenyl radical, and anion I$^-$ was examined first [69]. The Gibbs free energy required to transfer the electron from the cooper complexes to the iodobenzene is significantly high, i.e., +107.0, +118.1, and +120.2 kcal/mol for **2-NH**, **2-O** and **2-S**, respectively. The Gibbs energy barriers of this process were estimated using the Marcus-Hush theory [70–77] within the Saveant's

model [78–80] for the SET coupled with the cleavage of the Ph–I bond (see the Supplementary Materials pages S2–S4 for details) [51]. The activation barriers obtained are +116.0, +131.9, and +135.1 kcal/mol for **2-NH**, **2-O**, and **2-S**, respectively. A strong effect of the solvent is observed trigged by the stabilization of the iodine anion, as can be observed from entries 7 and 8 of Table 2.

Halogen Atom Transfer HAT has been suggested to govern the mechanism in the reaction of *O*- and *S*-arylations [59,60]. In this route, PhI transfers the iodine atom to the [(phen)Cu^{I}(XPh)] center leading to the formation of a complex [(phen)Cu^{I}(I)(XPh)]$^{\bullet}$ and a phenyl radical. The phenyl radical is attached then to the nucleophile moiety in [(phen)Cu^{I}(I)(XPh)]$^{\bullet}$ radical intermediate to form the coupling product (**3-X**). Our DFT calculations predict that the intermediates in the gas phase lie at 25.2, 27.0, and 31.2 kcal/mol when X is NH, O, and S, respectively. The calculations in toluene and acetonitrile as solvents estimate a stabilization between 1 kcal/mol and 3 kcal/mol for the intermediates. The results in toluene particularly indicate that the radicals formed are more stable that those reported by Houk et al. [51] and Zhang et al. [59,60], i.e., +43.0 kcal/mol for [(phen)Cu^{I}(I)(NHMe)]$^{\bullet}$, +34.0 kcal/mol for [(phen)Cu^{I}(I)(OMe)]$^{\bullet}$, +28.7 kcal/mol for [(phen)Cu^{I}(Br)(OPh)]$^{\bullet}$, +32.2 kcal/mol for [(phen)Cu^{I}(I)(SPh)]$^{\bullet}$. We estimated the barrier energy by the Marcus-Hush equation (see Supplementary Materials page S4), for all the reaction studied the HAT Gibbs activation energy is above 30 kcal/mol.

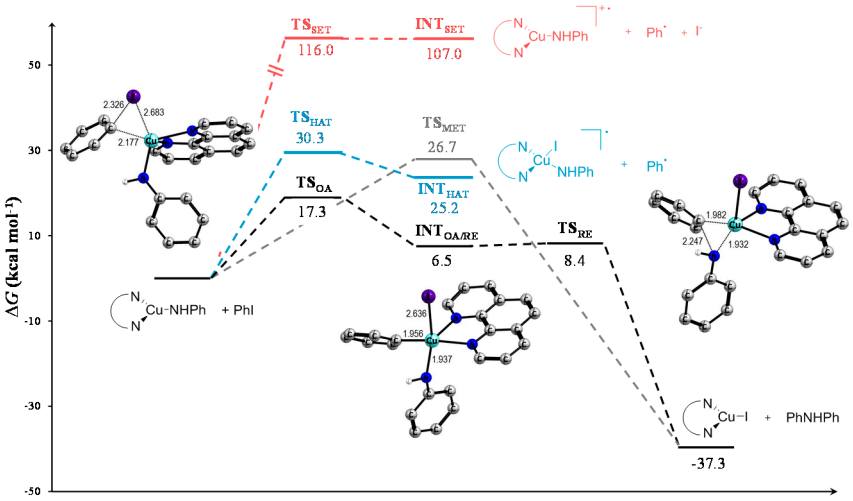

(**a**)

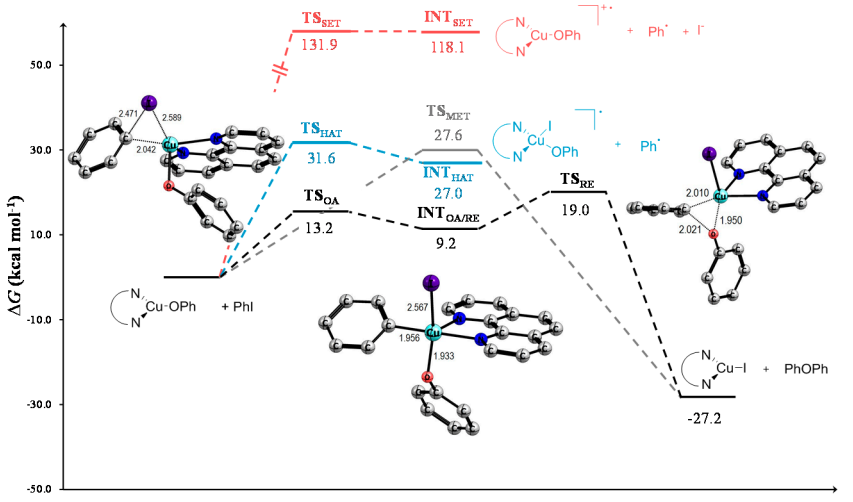

(**b**)

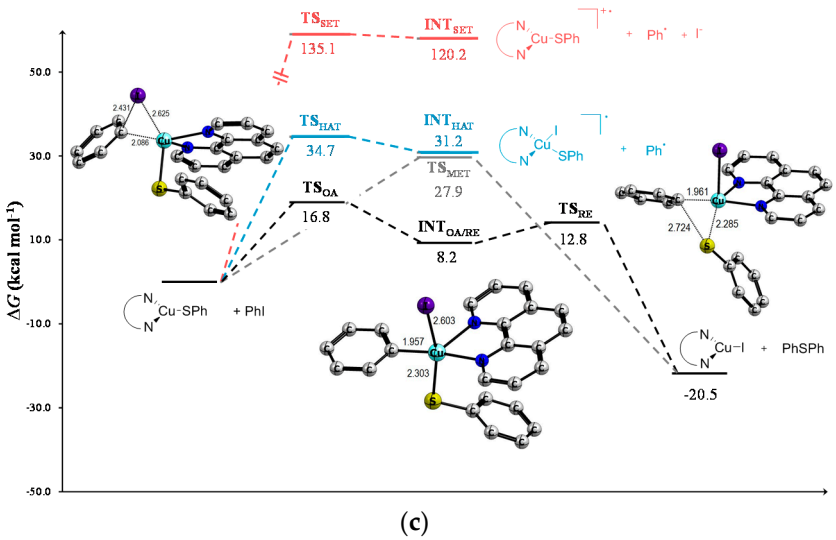

Figure 2. Computed Gibbs energy profile (Δ*G* [kcal/mol] at 298.15 K) at the B3LYP + D3(BJ)/def2-TZVPP//B3LYP/def2-SVP of the cooper-catalyzed cross-coupling reaction: (**a**) PhI (**1**) and aniline (**2-NH**); (**b**) PhI (**1**) and phenol (**2-O**); (**c**) PhI (**1**) and thiophenol (**2-S**). Oxidative Addition–Reductive Elimination (OA-RE) (—); Methatesis (MET) (—); Halogen Atom Transfer (HAT) (—) and Single Electron Transfer (SET) (—). The hydrogen atoms attached to carbon atoms are omitted for clarity.

The two-electron reaction mechanisms MET and OA-RE pathway were considered. On the one hand, the Transition State TS_{MET} consists in concerted $C_{(PhI)}$–I and Cu–X bond breaking and $C_{(PhI)}$–X and Cu–I bond formation. The congested four-membered transition states have high energy penalties as is reflected in the activation barriers, i.e., +26.7, +27.6, and +27.9 kcal/mol. The OA-RE route instead involves the same bond formation/cleavage but in two elementary steps. The first step is the oxidative addition and consists of the cleavage of the Ph-I bond via a three-membered transition state (TS_{OA}) to afford a five-coordinated copper(III) Intermediate [(phen)Cu^{III}(I)(Ph)(XPh)] ($INT_{OA/RE}$). The consecutive second step forms the final product Ph–X–Ph and the catalysts [(phen)Cu^{I}(I)] through TS_{RE}. The energies of all structures along the OA-RE pathway exhibited in Figure 2 reveal that this is the most favored reaction mechanism. The first transition state TS_{OA} is predicted to have relative Gibbs free energies in the gas phase of +17.3, +13.2, and +16.8 kcal/mol for the reaction with $PhNH_2$, PhOH, and PhSH, respectively. These transition states are strongly developed for *O*-arylation given the Cu–C bond length of 2.042 Å, while for *N*- and *S*-arylation the bond formation is less developed, i.e., Cu–C bond length 2.177 Å and 2.086 Å, respectively. The resulting intermediates [(phen)Cu^{III}(I)(Ph)(XPh)] are predicted to have Gibbs free energies of +6.5, +9.2, and +8.2 kcal/mol with respect to the reactants for *X* = NH, O, and S (in that order). The reductive elimination step is faster than the oxidative addition step for all the complexes studied. Thus, the energies needed to proceed from $INT_{OA/RE}$ are 1.9 (*X* = NH), 9.8 (*X* = O), and 4.6 (*X* = S) kcal/mol. The overall solvent effect increases the relative energies of the transition state and intermediate structures with respect to the reactants. This effect can be ascribed to the less polar nature of the intermediate structures in comparison with the reactant species.

Table 2. Gibbs Free Energies (kcal/mol) for Key Stationary Points (SP) in the mechanisms of Ullmann-Type *X*-Arylation Reactions (*X* = NH, O, S) in different solvents.[1]

Entry	SP	$PhNH_2$			PhOH			PhSH		
		ΔG_{gas}	ΔG_{tol}	ΔG_{acn}	ΔG_{gas}	ΔG_{tol}	ΔG_{acn}	ΔG_{gas}	ΔG_{tol}	ΔG_{acn}
1	TS_{OA}	17.3	18.9	20.4	13.2	15.5	17.0	16.8	19.0	20.5
2	$INT_{OA/RE}$	6.5	7.5	8.5	9.2	11.4	13.2	8.2	9.3	10.0
3	TS_{RE}	8.4	8.2	7.9	19.0	20.1	20.7	12.8	14.1	15.1
4	TS_{Met}	26.7	28.0	29.2	27.6	30.0	32.0	27.9	29.7	31.6

5	TS_{HAT}	30.3	29.5	32.6	31.6	31.8	35.1	34.7	34.6	37.7
6	INT_{HAT}	25.2	23.7	22.2	27.0	27.0	26.3	31.2	30.8	30.3
7	TS_{SET}	116.0	56.3	33.9	131.9	67.9	41.5	135.1	70.0	43.0
8	INT_{SET}	107.0	56.2	24.3	118.1	67.8	35.6	120.2	69.7	37.7
9	Prod	−37.3	−39.6	−40.9	−27.2	−28.2	−28.5	−20.5	−21.8	−22.1

[1] All calculations were computed at the PCM-[B3LYP + D3(BJ)/def2-TZVPP//B3LYP/def2-SVP] level of theory.

The overall results indicate that the copper-catalyzed cross-coupling reaction of *N*-, *O*-, and *S*-arylation undergoes an OA-RE reaction mechanism. These outcomes are in sharp contrast with the observations reported by Buchwald et al. [51] and Zhang et al. [59,60] where the operating mechanisms are the one-electron pathways HAT or SET. The energy barriers in toluene shown in Table 2 can be compared with those reported in the literature. Our values are in general lower than those informed before, to mention, the *N*-arylation of amide (+28.7 kcal/mol) [57], the *O*-arylation (+34.2 kcal/mol) [59], and the *S*-arylation (+39.3 kcal/mol) [60] reactions. Indeed, a direct comparison can be done with the last value shown which corresponds to the reaction between PhI and PhSH. The energy profiles recomputed with different functionals (B3LYP, M06, PBE0, TPSSh, PBE + D3(BJ) and TPSSh + D3(BJ) see Supplementary Materials, Tables S1–S6) led to small differences. It is noteworthy that the functionals without dispersion corrections give comparable energies between the HAT and the OA-RE pathways. However, those methods which include dispersion corrections estimate a significant reduction of the OA-RE energies. A similar effect was pointed out for similar copper-catalyzed reactions by Yu et al. [64] and Huang et al. [81]. In this regard, we recomputed copper-catalyzed Ullmann *O*-arylation of methanol studied by Houk and Buckwald (see Table S7 in the Supplementary Materials) [51]. The energy barrier of the HAT route remains comparable being +31.9 kcal/mol while the reported value is +34.0 kcal/mol [51]. Remarkable, in the case of the OA-RE route the energy barrier of the oxidative addition shows a significant reduction of about 25 kcal/mol. Our computed value is +18.8 kcal/mol while the reported one is +43.2 kcal/mol [51]. Such a strong effect of the dispersion corrections on transition states in different catalytic systems has been repeatedly observed and revisited [82,83].

Thermodynamics of the whole [(phen)Cu^{I}(XPh)] + **1** → **3-X** + [(phen)Cu^{I}I] conversion in the gas phase is favored by −37.3 kcal/mol for aniline, −27.2 kcal/mol for phenol, and −20.5 kcal/mol for thiophenol. When solvents are considered the conversions are more favored by around 1.3 to 3.6 kcal/mol. As the more feasible is the reaction mechanism OA-RE, to determine the rate-determining step in solution, we have to compare the Gibbs free energy differences of the [(phen)Cu^{I}(XPh)] + **1** → TS_{OA} and $INT_{OA/RE}$ → TS_{RE} steps. This is due to the fact that intermediates are stable enough in solution to be in thermal equilibrium with the environment. Therefore, in solution, the activation of PhI becomes the rate-determining step for all the cross-coupling calculated. These results are in agreement with the general kinetic observations [40,56]. Interestingly, the predicted activation energy barriers are consistent with the increasing reactivity trend NH (+4.2 kcal/mol) < S (+3.7 kcal/mol) < O (+0.2 kcal/mol).

To gain more quantitative insight into the above reactivity trends and the factors controlling the barrier heights for the oxidative additions, the Activation Strain Model (ASM, see Computational details) was applied. Figure 3 shows the activation strain diagrams (ASD) where the computed potential energy surfaces $\Delta E(\zeta)$ and its energy contributing terms along the Intrinsic Reaction Coordinate are drawn in this case over the Cu–C bond formation. The potential energy surface is dissected into the strain associated with deformation of the individual reactants ($\Delta E_{strain}(\zeta)$) and the instantaneous interaction between the deformed reactants ($\Delta E_{int}(\zeta)$). The ASDs nicely illustrate the effect of the nature of the heteroatom X on the oxidative addition step of the cross-coupling reactions. Thus, for the reaction involving [(phen)Cu^{I}(NHPh)], the strain energy increases smoothly from the beginning of the process and only becomes highly destabilizing close to the transition state ($\Delta E_{strain}^{\ddagger}$ = +30.4 kcal/mol). In addition, the interaction energy between the deformed reactants become strongly stabilizing at longer Cu–C bond distances ($\Delta E_{int}^{\ddagger}$ = −26.2 kcal/mol). As a result, a relatively high

activation barrier is computed at a relatively early stage of the process. In the same way, the reaction between **1** and [(phen)Cu^{I}(SPh)] has the same shape for the strain energy ($\Delta E_{strain}^{\ddagger}$ = +39.0 kcal/mol) but the interaction energy is less stabilizing than for the [(phen)Cu^{I}(NHPh)] complex. The interaction energy then results in being the dominant effect at a relatively advanced development of the Cu–C bond formation ($\Delta E_{int}^{\ddagger}$ = −35.3 kcal/mol). In the case of [(phen)Cu^{I}(OPh)], the strain energy varies more smoothly than its analogues, the stabilizing effect of the interaction term can compensate the strong destabilizing effect of the deformation energy ($\Delta E_{strain}^{\ddagger}$ = +36.6 kcal/mol vs. $\Delta E_{int}^{\ddagger}$ = −36.4 kcal/mol) only when the Cu–C is almost formed. Clearly, the controlling factor to give origin to the barrier height of the oxidative addition of PhI to [(phen)Cu^{I}(XPh)] is the energy needed to deform the reactants from their initial equilibrium geometries to the geometries they adopt in the corresponding transition state.

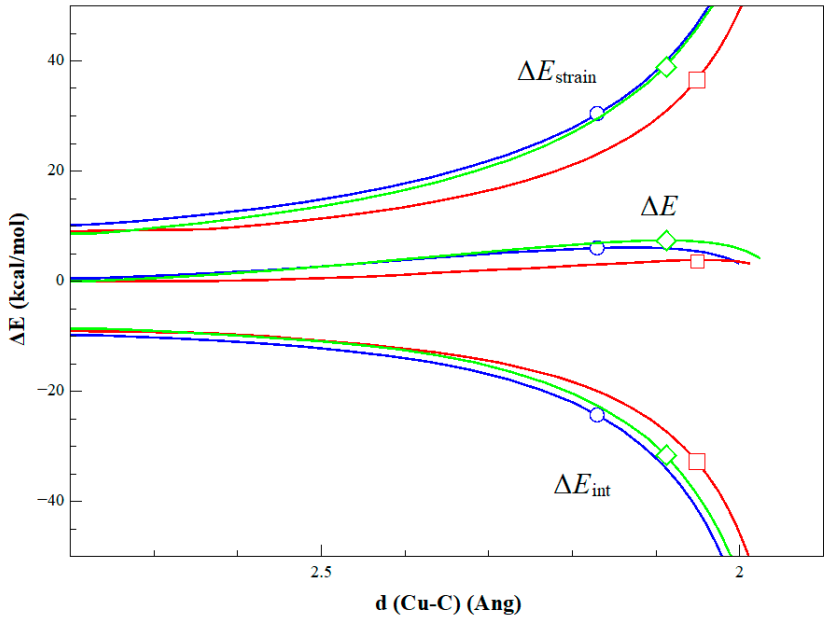

Figure 3. Activation Strain Model (ASM) diagram of the oxidative addition reaction of PhI (**1**) to [Cu(phen)XPh] where *X* = NH (blue curves), *X* = O (red curves), and *X* = S (green curves). The position of the corresponding TSs is indicated by a dot. All data were computed at the B3LYP + D3(BJ)/def2-TZVPP//B3LYP/def2-SVP level of theory.

Figure 4 displays the partitioning of the strain energy into contributions of each reactant. The diagrams indicate a different situation depending on the nature of the heteroatom. On the one hand, when X is NH the major contribution to the total strain energy is the deformation associated with the copper(I) complex ($\Delta E_{strain}^{\ddagger}$[(phen)Cu^{I}(NHPh)] = +17.6 kcal/mol vs. $\Delta E_{strain}^{\ddagger}$(PhI) = +12.7 kcal/mol). It is well-known, that such a change in the complex angle is required to achieve the maximum orbital overlap between the interacting orbitals of the fragments [84,85]. In this case, the occupied *d* orbital should interact with the σ*(C–I) vacant orbital. The $\Delta E_{strain}(\zeta)$ curve of the oxidative addition *N*-arylation is dominated by the deformation of the copper active complex at the begging of the process and it varies slightly along the intrinsic reaction coordinate (IRC). In contrast, the deformation of the [(phen)Cu^{I}(OPh)] and [(phen)Cu^{I}(SPh)] complexes costs about 2.1 kcal/mol less than the amido analogue. Thus, at the transition state the energy needed to deform the PhI is higher than to deform the complexes $\Delta E_{strain}^{\ddagger}$[(phen)Cu^{I}(OPh)] = +16.7 kcal/mol vs. $\Delta E_{strain}^{\ddagger}$(PhI) = +19.9 kcal/mol and $\Delta E_{strain}^{\ddagger}$[(phen)Cu^{I}(SPh)] = +16.3 kcal/mol vs. $\Delta E_{strain}^{\ddagger}$(PhI) = +19.7 kcal/mol. In these cases, the curves have a significant contribution by the deformation of the complex, whereas in the proximities of the transition state (Cu–C distance of ca. 2.11 Å) the deformation of PhI becomes prevalent.

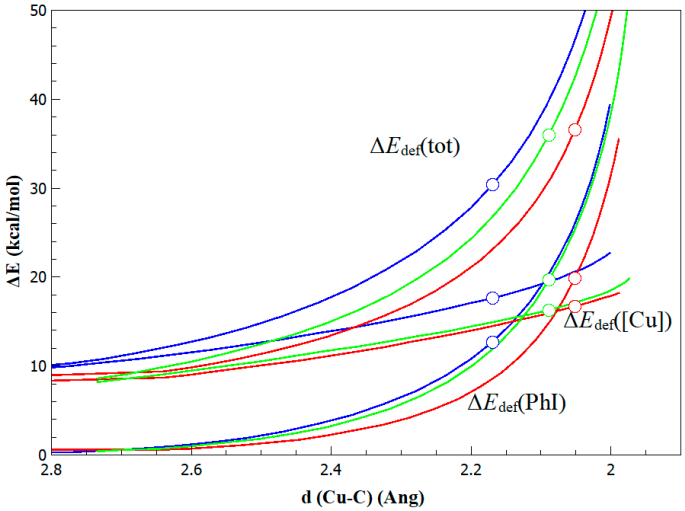

Figure 4. Contributions to the total strain energy along the reaction coordinate of the oxidative addition reaction of PhI (**1**) to [(phen)Cu^{I}(XPh)] where *X* = NH (blue curves), *X* = O (red curves), and *X* = S (green curves). The position of the corresponding TSs is indicated by a dot. All data were computed at the B3LYP + D3(BJ)/def2-TZVPP//B3LYP/def2-SVP level of theory.

Additionally, the interaction energy between the deformed reactants can be further analyzed within the energy decomposition analysis (EDA) framework. As graphically shown in Figure 5 for the oxidative addition in the *N*-arylation of aniline (Figures S1 and S2 for *O*-arylation and *S*-arylation, respectively), the main contribution to the total interaction between PhI and [(phen)Cu^{I}(NHPh)] comes from the electrostatic attraction. Indeed, the ΔE_{elst} term contributes around 52% to the total attraction in the transition state while the ΔE_{orb} and ΔE_{disp} terms do it with about 38% and 10%, respectively. The contribution of the orbital interaction term is very significant, and it is mainly the result of the 3*d*(Cu)-σ*(Ph–I) interaction. The absolute values for the electrostatic terms ($\Delta E_{elst}^{\ddagger}$) are −73.1, −93.7 and −95.1 kcal/mol for *X* = NH, O, and S, respectively, while the orbital term ($\Delta E_{orb}^{\ddagger}$) give −53.8, −71.7, and −68.8 kcal/mol in the same order. However, when these terms are compared at the same Cu–C bond distance, no real differences are observed. Although the nature of the heteroatom could affect the electronic feature of the metal center, no such change is reflected in the EDA analysis. The computed interactions between PhI and [(phen)Cu^{I}(XPh)] reactants are similar regardless of the nature of X after the copper complex is deformed. Therefore, our data suggest that the reactivity of the Ullmann type cross-coupling reactions are controlled by the energy needed to deform the reacting compounds.

It is worth mentioning that the ΔE_{disp} term is about ca. −15 kcal/mol stabilization at the transition state. This number counts the overestimation on the transition state energy of the OA-RE mechanism of the former DFT studies.

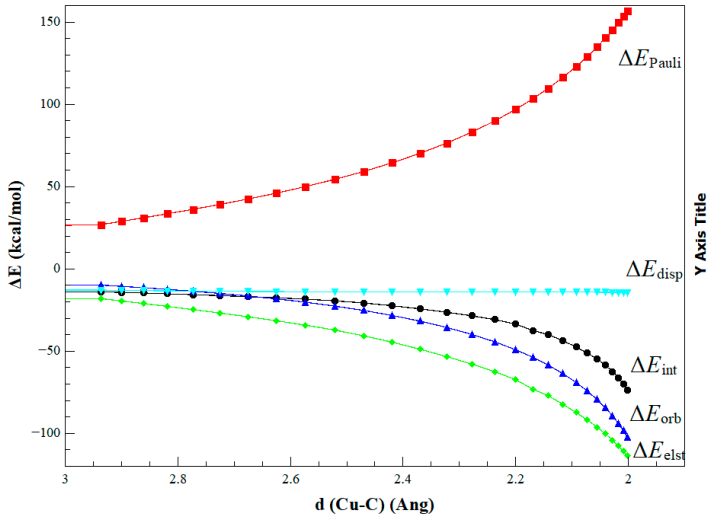

Figure 5. Energy decomposition analysis (EDA) of the interaction energy for the oxidative addition reaction of PhI (**1**) to [(phen)Cu^{I}(NHPh)] projected onto the forming Cu–C bond. All data were computed at the BP86 + D3(BJ)/TZ2P +//B3LYP/def2-SVP level.

3. Computational Details

All geometries were optimized without symmetry constraint within the DFT (density functional theory) framework using the B3LYP functional [86,87] in combination with the Ahlrichs def2-SVP basis function [88]. These calculations were performed using the Gaussian 09 optimizer (Gaussian 09, Revision D.01, Gaussian, Inc., Wallingford, CT, USA, 2013) [89] together with TurboMole V6.0 (TURBOMOLE GmbH, Karlsruhe, Germany, 2007) [90]. The stationary points were located with the Berny algorithm [91] using redundant internal coordinates. Analytical Hessians were computed to determine the nature of stationary points (one and zero imaginary frequencies for transition states and minima, respectively) [92] and to calculate unscaled zero-point energies (ZPEs) as well as thermal corrections and entropy effects using the standard statistical-mechanics relationships for an ideal gas [93]. Transition structures (TSs) show only one negative eigenvalue in their diagonalized force constant matrices, and their associated eigenvectors were confirmed to correspond to the motion along the reaction coordinate under consideration using the intrinsic reaction coordinate (IRC) method [94]. The electronic energies were improved by single point calculations at the B3LYP + D3(BJ)/def2-TZVPP [95,96] level of theory. For comparison additional calculations were performed at M06/def2-TZVPP [97], TSPPh/def2-TZVPP [98,99], TSPP + D3(BJ)/def2-TVPP[100], PBE0/def2-TZVPP [101], and PBE + D3(BJ)/def2-TZVPP (see Supplementary Materials) [102,103]. Unless otherwise stated, Gibbs energies were computed at 298.15 K. For these calculations the toluene and acetonitrile solvents were described by nonspecific solvent effects within the self-consistent reaction field (SCRF) approach in Tomasi's formalism [104,105].

The Wiberg Bond Indices [106] and NPA [107,108] atomic partial charges were calculated at the B3LYP + D3(BJ)/def2-TZVPP//B3LYP/def2-SVP level of theory using GAUSSIAN 09 (Gaussian 09, Revision D.01, Gaussian, Inc., Wallingford, CT, USA, 2013) [89] and GENNBO5.9 programs (Theoretical Chemistry Institute, University of Wisconsin, Madison, WI, USA, 2009) [109].

The origins of the reaction barriers were studied by the so-called Activation-Strain Model of reaction profiles (ASM) [110], also known as distortion/interaction model [111]. This model consists of a systematic extension of the fragment approach from the equilibrium structures to the transition state as well as the nonstationary point along the intrinsic reaction coordinate. Thus, within this approach the potential energy surface $\Delta E(\zeta)$ is dissected, along the reaction coordinate ζ, into the strain or deformation $\Delta E_{strain}(\zeta)$ related to the energy needed to deform the individual fragments, and the interaction energy $\Delta E_{int}(\zeta)$ between these deformed moieties Equation (1)

$$\Delta E(\zeta) = \Delta E_{strain}(\zeta) + \Delta E_{\text{int}}(\zeta) \quad (1)$$

The term $\Delta E_{strain}(\zeta)$ is associated with the rigidity of the reactants and the extent to which the group should reorganize such that the reaction step can occur, while the term $\Delta E_{int}(\zeta)$ accounts for the strength of the interaction between the fragments depending on their mutual orientation and electronic structure. Overall, the interplay between these two terms leads to the point along the ζ where the transition state arises. In the specific cases studied here the copper–carbon (Cu–C) bond formation was taken as the reaction coordinate.

Additionally, the interaction energy can be separated in the light of the Energy Decomposition Analysis (EDA) method, which was developed by Morokuma [112] and by Ziegler and Rauk [113,114]. The bonding analysis focuses on the instantaneous interaction energy ΔE_{int} of a bond A–B between two fragments A and B in the particular electronic reference state and in the frozen geometry AB. This energy is divided into four main components (Equation (2)).

$$\Delta E_{\text{int}} = \Delta E_{elst} + \Delta E_{Pauli} + \Delta E_{orb} + \Delta E_{disp} \quad (2)$$

The term ΔE_{elst} corresponds to the classical electrostatic interaction between the unperturbed charge distributions of the prepared atoms (or fragments) and it is usually attractive. The Pauli repulsion ΔE_{Pauli} is the energy change associated with the transformation from the superposition of the unperturbed wave functions (Slater determinant of the Kohn-Sham orbitals) of the isolated fragments to the wave function $\Psi_0 = N\hat{A}[\Psi_A\Psi_B]$, which properly obeys the Pauli principle through explicit antisymmetrization ($\hat{A}$ operator) and renormalization (N = constant) of the product wave function. It comprises the destabilizing interactions between electrons of the same spin on either fragment. The orbital interaction ΔE_{orb} accounts for charge transfer and polarization effects [115]. In the case when the Grimme dispersion corrections [95,96] are computed, the term ΔE_{disp} is added to Equation (2). Further details on the EDA method [116,117] and ASM applications to the analysis of the chemical reactions can be found in the literature [118,119].

Herein, the basis sets for all elements have triple-ζ quality augmented by two sets of polarizations functions and one set of diffuse function. Core electrons were treated by the frozen-core approximation. This level of theory is denoted BP86 + D3(BJ)/TZ2P+ [120]. Scalar relativistic effects were incorporated by applying the zeroth-order regular approximation (ZORA) [121].

4. Conclusions

From the computational study reported in this paper, the following conclusions can be drawn: (i) the copper-catalyzed Ullmann-type *N*-, *O*-, and *S*-arylation cross-coupling reactions take place via oxidative addition—reductive elimination mechanism through penta-coordinated Cu^{III} intermediates. (ii) In good agreement with the experimental findings, the oxidative addition of iodobenzene to active copper complexes [(phen)Cu^{I}(XPh)] is the rate-determining step. (iii) The polarity of the solvent increases the relative energy of the intermediate structures in the OA-RE pathway given their less polar nature. (iv) The reactivity is reduced by changing the heteroatom nature following the order X = O > S > NH. (v) This trend in the oxidative addition is controlled by the strain energy associated with the deformation of the reactants from their equilibrium geometries to the geometries they adopt in the transition state. The differences observed are mainly ascribed to the [(phen)Cu^{I}(XPh)] geometry change.

Supplementary Materials: Cartesian coordinates (in Å) and total energies (in a.u., noncorrected zero-point vibrational energies included) of all the stationary points discussed in the text are available online at www.mdpi.com/2073-4344/7/12/388/s1. Table S1: Gibbs Free Energies (kcal/mol) for Key Stationary Points in the Mechanisms of Ullmann-Type *X*-Arylation Reactions (*X* = NH, O, S) in different solvents at the PCM-[B3LYP/def2-TZVPP//B3LYP/def2-SVP] level of theory, Table S2: Gibbs Free Energies (kcal/mol) for Key Stationary Points in the Mechanisms of Ullmann-Type *X*-Arylation Reactions (*X* = NH, O, S) in different solvents at the PCM-[M06/def2-TZVPP//B3LYP/def2-SVP] level of theory, Table S3: Gibbs Free Energies (kcal/mol) for Key Stationary Points in the Mechanisms of Ullmann-Type *X*-Arylation Reactions (*X* = NH, O, S) in different solvents at the PCM-[TPSSh/def2-TZVPP//B3LYP/def2-SVP] level of theory, Table S4: Gibbs Free Energies

(kcal/mol) for Key Stationary Points in the Mechanisms of Ullmann-Type *X*-Arylation Reactions (*X* = NH, O, S) in different solvents at the PCM-[TPSS + D3(BJ)/def2-TZVPP//B3LYP/def2-SVP] level of theory, Table S5: Gibbs Free Energies (kcal/mol) for Key Stationary Points in the Mechanisms of Ullmann-Type *X*-Arylation Reactions (*X* = NH, O, S) in different solvents at the PCM-[PBE/def2-TZVPP//B3LYP/def2-SVP] level of theory, Table S6: Gibbs Free Energies (kcal/mol) for Key Stationary Points in the Mechanisms of Ullmann-Type *X*-Arylation Reactions (*X* = NH, O, S) in different solvents at the PCM-[PBE + D3(BJ)/def2-TZVPP//B3LYP/def2-SVP] level of theory, Figure S1: EDA of the interaction energy for the oxidative addition reaction of PhI (**1**) to [(phen)CuI(OPh)] projected onto the forming Cu–C bond. All data have been computed at the BP86 + D3(BJ)/TZ2P+//B3LYP/def2-SVP level, Figure S2: EDA of the interaction energy for the oxidative addition reaction of PhI (**1**) to [(phen)CuI(SPh)] projected onto the forming Cu–C bond. All data have been computed at the BP86 + D3(BJ)/TZ2P+//B3LYP/def2-SVP level.

Acknowledgments: This work was supported by the Universität des Saarlandes. The work at Córdoba was supported by CONICET, Agencia Nacional de Promoción Científica y Técnica (ANPCyT) and SeCyT-UNC.

Author Contributions: D.M.A. conceived, performed the calculations, analyzed the data, and wrote the paper. S.M.S.-C., D.A.C., J.E.A., and A.B.P. analyzed the data and wrote the paper.

Conflicts of Interest: The authors declare no conflict of interest.

References and Notes

1. Beletskaya, I.P.; Cheprakov, A.V. Copper in cross-coupling reactions—The post-Ullmann chemistry. *Coord. Chem. Rev.* **2004**, *248*, 2337–2364.
2. Beletskaya, I.P.; Ananikov, V.P. Transition-metal-catalyzed C–S, C–Se, and C–Te bond formation via cross-coupling and atom-economic addition reactions. *Chem. Rev.* **2011**, *111*, 1596–1636.
3. Evano, G.; Theunissen, C.; Pradal, A. Impact of Copper-catalyzed cross-coupling reactions in natural product synthesis: The emergence of new retrosynthetic paradigms. *Nat. Prod. Rep.* **2013**, *30*, 1467–1489.
4. Sambiagio, C.; Marsden, S.P.; Blacker, A.J.; McGowan, P.C. Copper catalysed Ullmann type chemistry: From mechanistic aspects to modern development. *Chem. Soc. Rev.* **2014**, *43*, 3525–3550.
5. Monnier, F.; Taillefer, M. Catalytic C–C, C–N, and C–O Ullmann-type coupling reactions. *Angew. Chem. Int. Ed.* **2009**, *48*, 6954–6971.
6. Bhunia, S.; Pawar, G.G.; Kumar, S.V.; Jiang, Y.; Ma, D. Selected copper-based reactions for C−N, C−O, C−S, and C-C bond formation. *Angew. Chem. Int. Ed.* **2017**, doi:10.1002/anie.201701690.
7. Ullmann, F.; Bielecki, J. Ueber synthesen in der biphenylreihe. *Ber. Dtsch. Chem. Ges.* **1901**, *34*, 2174–2185.
8. Ullmann, F. Ueber eine neue bildungsweise von diphenylaminderivaten. *Ber. Dtsch. Chem. Ges.* **1903**, *36*, 2382–2384.
9. Ullmann, F.; Sponagel, P. Ueber die phenylirung von phenolen. *Ber. Dtsch. Chem. Ges.* **1905**, *38*, 2211–2212.
10. Goldberg, I. Ueber phenylirungen bei gegenwart von kupfer als katalysator. *Ber. Dtsch. Chem. Ges.* **1906**, *39*, 1691–1692.
11. Lindley, J. Tetrahedron report number 163: Copper assisted nucleophilic substitution of aryl halogen. *Tetrahedron* **1984**, *40*, 1433–1456.
12. Monnier, F.; Taillefer, M. Catalytic C–C, C–N, and C–O Ullmann-type coupling reactions: Copper makes a difference. *Angew. Chem. Int. Ed.* **2008**, *47*, 3096–3099.
13. Surry, D.S.; Buchwald, S.L. Diamine ligands in Copper-catalyzed reactions. *Chem. Sci.* **2010**, *1*, 13–31.
14. Goodbrand, H.B.; Hu, N.X. Ligand-accelerated catalysis of the Ullmann condensation: Application to hole conducting triarylamines. *J. Org. Chem.* **1999**, *64*, 670–674.
15. Gujadhur, R.; Venkataraman, D.; Kintigh, J.T. Formation of aryl-nitrogen bonds using a soluble Copper(I) catalyst. *Tetrahedron Lett.* **2001**, *42*, 4791–4793.
16. Gujadhur, R.K.; Bates, C.G.; Venkataraman, D. Formation of aryl-nitrogen, aryl-oxygen, and aryl-carbon bonds using well-defined Copper(I)-based catalysts. *Org. Lett.* **2001**, *3*, 4315–4317.
17. Han, C.; Shen, R.C.; Su, S.; Porco, J.A. Copper-mediated synthesis of *N*-acyl vinylogous carbamic acids and derivatives: Synthesis of the antibiotic CJ-15,801. *Org. Lett.* **2004**, *6*, 27–30.
18. Wolter, M.; Klapars, A.; Buchwald, S.L. Synthesis of *N*-aryl hydrazides by copper-catalyzed coupling of hydrazides with aryl iodides. *Org. Lett.* **2001**, *3*, 3803–3805.
19. Klapars, A.; Huang, X.H.; Buchwald, S.L. A general and efficient Copper catalyst for the amidation of aryl halides. *J. Am. Chem. Soc.* **2002**, *124*, 7421–7428.

20. Kwong, F.Y.; Buchwald, S.L. Mild and efficient Copper-catalyzed amination of aryl bromides with primary alkylamines. *Org. Lett.* **2003**, *5*, 793–796.
21. Kwong, F.Y.; Klapars, A.; Buchwald, S.L. Copper-catalyzed coupling of alkylamines and aryl iodides: An efficient system even in an air atmosphere. *Org. Lett.* **2002**, *4*, 581–584.
22. Ma, D.; Cai, Q. Copper/amino acid catalyzed cross-couplings of aryl and vinyl halides with nucleophiles. *Acc. Chem. Res.* **2008**, *41*, 1450–1460.
23. Zhang, H.; Cai, Q.; Ma, D.W. Amino acid promoted cui-catalyzed C-N bond formation between aryl halides and amines or *N*-containing heterocycles. *J. Org. Chem.* **2005**, *70*, 5164–5173.
24. Deng, W.; Wang, Y.F.; Zou, W.; Liu, L.; Guo, Q.X. Amino acid-mediated Goldberg reactions between amides and aryl iodides. *Tetrahedron Lett.* **2004**, *45*, 2311–2315.
25. Shafir, A.; Buchwald, S.L. Highly selective room-temperature Copper-catalyzed C–N coupling reactions. *J. Am. Chem. Soc.* **2006**, *128*, 8742–8743.
26. Shafir, A.; Lichtor, P.A.; Buchwald, S.L. *N*- versus *O*-arylation of aminoalcohols: Orthogonal selectivity in Copper-based catalysts. *J. Am. Chem. Soc.* **2007**, *129*, 3490–3491.
27. Cristau, H.J.; Cellier, P.P.; Spindler, J.F.; Taillefer, M. Highly efficient and mild Copper-catalyzed *N*- and *C*-arylations with aryl bromides and iodides. *Chem. Eur. J.* **2004**, *10*, 5607–5622.
28. Fagan, P.J.; Hauptman, E.; Shapiro, R.; Casalnuovo, A. Using intelligent/random library screening to design focused libraries for the optimization of homogeneous catalysts: Ullmann ether formation. *J. Am. Chem. Soc.* **2000**, *122*, 5043–5051.
29. Chen, Y.-J.; Chen, H.-H. 1,1,1-tris(hydroxymethyl)ethane as a new, efficient, and versatile tripod ligand for Copper-catalyzed cross-coupling reactions of aryl iodides with amides, thiols, and phenols. *Org. Lett.* **2006**, *8*, 5609–5612.
30. Shen, R.C.; Porco, J.A. Synthesis of enamides related to the salicylate antitumor macrolides using copper-mediated vinylic substitution. *Org. Lett.* **2000**, *2*, 1333–1336.
31. Ley, S.V.; Thomas, A.W. Modern synthetic methods for copper-mediated C(aryl)–O, C(aryl)–N, and C(aryl)-S bond formation. *Angew. Chem. Int. Ed.* **2003**, *42*, 5400–5449.
32. Zweig, J.E.; Kim, D.E.; Newhouse, T.R. Methods utilizing first-row transition metals in natural product total synthesis. *Chem. Rev.* **2017**, *117*, 11680–11752.
33. Evano, G.; Blanchard, N.; Toumi, M. Copper-mediated coupling reactions and their applications in natural products and designed biomolecules synthesis. *Chem. Rev.* **2008**, *108*, 3054–3131.
34. Walsh, C.T. The chemical versatility of natural-product assembly lines. *Acc. Chem. Res.* **2008**, *41*, 4–10.
35. Murphy, A.R.; Frechet, J.M.J. Organic semiconducting oligomers for use in thin film transistors. *Chem. Rev.* **2007**, *107*, 1066–1096.
36. Daprano, G.; Leclerc, M.; Zotti, G.; Schiavon, G. Synthesis and characterization of polyaniline derivatives—Poly(2-alkoxyanilines) and poly(2,5-dialkoxyanilines). *Chem. Mater.* **1995**, *7*, 33–42.
37. Casitas, A.; King, A.E.; Parella, T.; Costas, M.; Stahl, S.S.; Ribas, X. Direct observation of Cu-I/Cu-III redox steps relevant to Ullmann-type coupling reactions. *Chem. Sci.* **2010**, *1*, 326–330.
38. Casitas, A.; Ribas, X. Insights into the mechanism of modern Ullmann–Goldberg coupling reactions. In *Copper-Mediated Cross-Coupling Reactions*; John Wiley & Sons, Inc.: New York, NY, USA, 2013; pp. 253–279.
39. Oxidation potentials for Cu(I)/Cu(0), $E°$ = 0.52 V; Cu(II)/Cu(I), $E°$ = 0.162 V, vs. SCE.
40. Giri, R.; Hartwig, J.F. Cu(I)-amido complexes in the Ullmann reaction: Reactions of Cu(I)-amido complexes with iodoarenes with and without autocatalysis by Cu(I). *J. Am. Chem. Soc.* **2010**, *132*, 15860–15863.
41. Bowman, W.R.; Heaney, H.; Smith, P.H.G. Copper(1) catalyzed aromatic nucleophilic-substitution—A mechanistic and synthetic comparison with the SRN1 reaction. *Tetrahedron Lett.* **1984**, *25*, 5821–5824.
42. Chen, C.H.; Weng, Z.Q.; Hartwig, J.F. Synthesis of Copper(I) thiolate complexes in the thioetherification of aryl halides. *Organometallics* **2012**, *31*, 8031–8036.
43. Furuta, H.; Maeda, H.; Osuka, A. Doubly n-confused porphyrin: A new complexing agent capable of stabilizing higher oxidation states. *J. Am. Chem. Soc.* **2000**, *122*, 803–807.
44. Ribas, X.; Jackson, D.A.; Donnadieu, B.; Mahia, J.; Parella, T.; Xifra, R.; Hedman, B.; Hodgson, K.O.; Llobet, A.; Stack, T.D.P. Aryl c-h activation by Cu(II) to form an organometallic aryl-Cu(III) species: A novel twist on copper disproportionation. *Angew. Chem. Int. Ed.* **2002**, *41*, 2991–2994.
45. Xifra, R.; Ribas, X.; Llobet, A.; Poater, A.; Duran, M.; Sola, M.; Stack, T.D.P.; Benet-Buchholz, J.; Donnadieu, B.; Mahia, J.; et al. Fine-tuning the electronic properties of highly stable organometallic Cu-III complexes containing monoanionic macrocyclic ligands. *Chem. Eur. J.* **2005**, *11*, 5146–5156.

46. Casitas, A.; Canta, M.; Sola, M.; Costas, M.; Ribas, X. Nucleophilic aryl fluorination and aryl halide exchange mediated by a Cu-I/Cu-III catalytic cycle. *J. Am. Chem. Soc.* **2011**, *133*, 19386–19392.
47. Huffman, L.M.; Stahl, S.S. Carbon-nitrogen bond formation involving well-defined aryl-Copper(III) complexes. *J. Am. Chem. Soc.* **2008**, *130*, 9196–9197.
48. Huffman, L.M.; Casitas, A.; Font, M.; Canta, M.; Costas, M.; Ribas, X.; Stahl, S.S. Observation and mechanistic study of facile C-O bond formation between a well-defined aryl-Copper(III) complex and oxygen nucleophiles. *Chem. Eur. J.* **2011**, *17*, 10643–10650.
49. Bacon, R.G.R.; Hill, H.A.O. Metal ions + complexes in organic reactions.I. Substitution reactions between aryl halides + cuprous salts in organic solvents. *J. Chem. Soc.* **1964**, 1097–1107, doi:10.1039/JR9640001097.
50. Bacon, R.G.R.; Karim, A. Metal-ions and complexes in organic reactions 15. Copper-catalyzed substitutions of aryl halides by phthalimide ion. *J. Chem. Soc. Perkin Trans.* **1973**, *1*, 272–278.
51. Jones, G.O.; Liu, P.; Houk, K.N.; Buchwald, S.L. Computational explorations of mechanisms and ligand-directed selectivities of Copper-catalyzed Ullmann-type reactions. *J. Am. Chem. Soc.* **2010**, *132*, 6205–6213.
52. Strieter, E.R.; Blackmond, D.G.; Buchwald, S.L. The role of chelating diamine ligands in the Goldberg reaction: A kinetic study on the Copper-catalyzed amidation of aryl iodides. *J. Am. Chem. Soc.* **2005**, *127*, 4120–4121.
53. Strieter, E.R.; Bhayana, B.; Buchwald, S.L. Mechanistic studies on the Copper-catalyzed *N*-arylation of amides. *J. Am. Chem. Soc.* **2009**, *131*, 78–88.
54. Wolter, M.; Nordmann, G.; Job, G.E.; Buchwald, S.L. Copper-catalyzed coupling of aryl iodides with aliphatic alcohols. *Org. Lett.* **2002**, *4*, 973–976.
55. Nordmann, G.; Buchwald, S.L. A domino copper-catalyzed C–O coupling-claisen rearrangement process. *J. Am. Chem. Soc.* **2003**, *125*, 4978–4979.
56. Tye, J.W.; Weng, Z.; Johns, A.M.; Incarvito, C.D.; Hartwig, J.F. Copper complexes of anionic nitrogen ligands in the amidation and imidation of aryl halides. *J. Am. Chem. Soc.* **2008**, *130*, 9971–9983.
57. Zhang, S.-L.; Liu, L.; Fu, Y.; Guo, Q.-X. Theoretical study on Copper(I)-catalyzed cross-coupling between aryl halides and amides. *Organometallics* **2007**, *26*, 4546–4554.
58. Zhang, S.L.; Ding, Y.Q. Theoretical study on mechanism of Copper(I)-catalyzed cross-coupling between aryl halides and alkylamines. *Organometallics* **2011**, *30*, 633–641.
59. Zhang, S.; Zhu, Z.; Ding, Y. Proposal for halogen atom transfer mechanism for Ullmann *O*-arylation of phenols with aryl halides. *Dalton Trans.* **2012**, *41*, 13832–13840.
60. Zhang, S.-L.; Fan, H.-J. Theoretical study on copper-catalyzed *S*-arylation of thiophenols with aryl halides: Evidence supporting the LCu(I)-SPh active catalyst and halogen atom transfer mechanism. *Organometallics* **2013**, *32*, 4944–4951.
61. Zhang, S.L.; Bie, W.F.; Huang, L. Theoretical insights into mechanisms for Copper(I)-catalyzed C–P coupling of diarylphosphines with aryl halides: A combined solvent and ancillary ligand effect on the identity of active catalyst and reaction mechanism. *Organometallics* **2014**, *33*, 5263–5271.
62. Soria-Castro, S.M.; Penenory, A.B. Efficient Cu-catalyzed base-free C-S coupling under conventional and microwave heating. A simple access to *S*-heterocycles and sulfides. *Beilstein J. Org. Chem.* **2013**, *9*, 467–475.
63. Soria-Castro, S.M.; Andrada, D.M.; Caminos, D.A.; Argüello, J.E.; Robert, M.; Peñéñory, A.B. Mechanistic insight into the Cu-catalyzed C–S cross-coupling of thioacetate with aryl halides: A joint experimental–computational study. *J. Org. Chem.* **2017**, *82*, 11464–11473.
64. Yu, H.-Z.; Jiang, Y.-Y.; Fu, Y.; Liu, L. Alternative mechanistic explanation for ligand-dependent selectivities in Copper-catalyzed *N*- and *O*-arylation reactions. *J. Am. Chem. Soc.* **2010**, *132*, 18078–18091.
65. Rout, L.; Saha, P.; Jammi, S.; Punniyamurthy, T. Efficient Copper(I)-catalyzed C–S cross coupling of thiols with aryl halides in water. *Eur. J. Org. Chem.* **2007**, 640–643, doi:10.1002/ejoc.200700978.
66. Fiaschi, P.; Floriani, C.; Pasquali, M.; Chiesivilla, A.; Guastini, C. Copper(I) phenoxide complexes—Synthesis and ligand-induced transformations of the Copper(I) phenoxo functionality. *Inorg. Chem.* **1986**, *25*, 462–469.
67. Tye, J.W.; Weng, Z.Q.; Giri, R.; Hartwig, J.F. Copper(I) phenoxide complexes in the etherification of aryl halides. *Angew. Chem. Int. Ed.* **2010**, *49*, 2185–2189.
68. Stange, A.F.; Sixt, T.; Kaim, W. Highly dissymmetric chelate coordination of 3,4,7,8-tetramethyl-1, 10-phenanthroline to Cu-I(SR). *Chem. Comm.* **1998**, 469–470, doi:10.1039/A708867A.
69. We considered only the outer-sphere set mechanism. The inner-sphere set mechanism was not possible to compute since we could not find any stable complex between [(phen)Cu^{I}(XPh)] and PhI.

70. Marcus, R.A. Theory of oxidation-reduction reactions involving electron transfer .3. Applications to data on the rates of organic redox reactions. *J. Chem. Phys.* **1957**, *26*, 872–877.
71. Marcus, R.A. On the theory of electrochemical and chemical electron transfer processes. *Can. J. Chem.* **1959**, *37*, 155–163.
72. Marcus, R.A. Chemical + electrochemical electron-transfer theory. *Annu. Rev. Phys. Chem.* **1964**, *15*, 155–196.
73. Marcus, R.A. On theory of electron-transfer reactions .6. Unified treatment for homogeneous and electrode reactions. *J. Chem. Phys.* **1965**, *43*, 679.
74. Marcus, R.A. The 2nd Robinson, R.A. Memorial lecture—Electron, proton and related transfers. *Faraday Discuss.* **1982**, *74*, 7–15.
75. Marcus, R.A.; Sutin, N. Electron transfers in chemistry and biology. *Biochim. Biophys. Acta* **1985**, *811*, 265–322.
76. Marcus, R.A. On the theory of oxidation-reduction reactions involving electron transfer. 1. *J. Chem. Phys.* **1956**, *24*, 966–978.
77. Marcus, R.A. Electrostatic free energy and other properties of states having nonequilibrium polarization. 1. *J. Chem. Phys.* **1956**, *24*, 979–989.
78. Saveant, J.M. A simple-model for the kinetics of dissociative electron-transfer in polar-solvents—Application to the homogeneous and heterogeneous reduction of alkyl-halides. *J. Am. Chem. Soc.* **1987**, *109*, 6788–6795.
79. Saveant, J.M. Dissociative electron-transfer—New tests of the theory in the electrochemical and homogeneous reduction of alkyl-halides. *J. Am. Chem. Soc.* **1992**, *114*, 10595–10602.
80. Saveant, J.M. Electron-transfer, bond breaking, and bond formation. *Acc. Chem. Res.* **1993**, *26*, 455–461.
81. Huang, W.K.; Chen, W.T.; Hsu, I.J.; Han, C.C.; Shyu, S.G. Cross C–S coupling reaction catalyzed by Copper(I) *N*-heterocyclic carbene complexes. *RSC Adv.* **2017**, *7*, 4912–4920.
82. Armstrong, A.; Boto, R.A.; Dingwall, P.; Contreras-Garcia, J.; Harvey, M.J.; Mason, N.J.; Rzepa, H.S. The Houk-list transition states for organocatalytic mechanisms revisited. *Chem. Sci.* **2014**, *5*, 2057–2071.
83. Kruse, H.; Goerigk, L.; Grimme, S. Why the standard B3LYP/6–31G* model chemistry should not be used in DFT calculations of molecular thermochemistry: Understanding and correcting the problem. *J. Org. Chem.* **2012**, *77*, 10824–10834.
84. Wolters, L.P.; van Zeist, W.-J.; Bickelhaupt, F.M. New concepts for designing d(10)-M(L)(N) catalysts: D regime, s regime and intrinsic bite-angle flexibility. *Chem. Eur. J.* **2014**, *20*, 11370–11381.
85. Hering, F.; Nitsch, J.; Paul, U.; Steffen, A.; Bickelhaupt, F.M.; Radius, U. Bite-angle bending as a key for understanding group-10 metal reactivity of d(10)-M(NHC)(2) complexes with sterically modest NHC ligands. *Chem. Sci.* **2015**, *6*, 1426–1432.
86. Becke, A.D. Density-functional thermochemistry. III. The role of exact exchange. *J. Chem. Phys.* **1993**, *98*, 5648–5652.
87. Lee, C.; Yang, W.; Parr, R.G. Development of the Colle-Salvetti correlation-energy formula into a functional of the electron density. *Phys. Rev. B* **1988**, *37*, 785–789.
88. Weigend, F.; Ahlrichs, R. Balanced basis sets of split valence, triple zeta valence and quadruple zeta valence quality for H to Rn: Design and assessment of accuracy. *Phys. Chem. Chem. Phys.* **2005**, *7*, 3297–3305.
89. Frisch, M.J.; Trucks, G.W.; Schlegel, H.B.; Scuseria, G.E.; Robb, M.A.; Cheeseman, J.R.; Scalmani, G.; Barone, V.; Mennucci, B.; Petersson, G.A.; et al. *Gaussian 09, Revision D.01*; Gaussian, Inc.: Wallingford, CT, USA, 2009.
90. Turbomole GmbH. *Turbomole Version 6.0 2015*; a Development of University of Karlsruhe and Forschungszentrum Karlsruhe GmbH, 1989–2007; TURBOMOLE GmbH: Karlsruhe, Germany, 2007. Available online: http://www.turbomole.com (accessed on 12 December 2017).
91. Peng, C.Y.; Ayala, P.Y.; Schlegel, H.B.; Frisch, M.J. Using redundant internal coordinates to optimize equilibrium geometries and transition states. *J. Comput. Chem.* **1996**, *17*, 49–56.
92. McIver, J.W.; Komornic, A. Structure of transition-states in organic reactions—General theory and an application to cyclobutene-butadiene isomerization using a semiempirical molecular-orbital method. *J. Am. Chem. Soc.* **1972**, *94*, 2625–2633.
93. Atkins, P.W.; De Paula, J. *Physical Chemistry*, 8th ed.; Oxford University Press: Oxford, NY, USA, 2006.
94. Gonzalez, C.; Schlegel, H.B. Reaction-path following in mass-weighted internal coordinates. *J. Phys. Chem.* **1990**, *94*, 5523–5527.
95. Grimme, S.; Antony, J.; Ehrlich, S.; Krieg, H. A consistent and accurate ab initio parametrization of density functional dispersion correction (DFT-D) for the 94 elements H-Pu. *J. Chem. Phys.* **2010**, *132*, 154104.

96. Grimme, S.; Ehrlich, S.; Goerigk, L. Effect of the damping function in dispersion corrected density functional theory. *J. Comput. Chem.* **2011**, *32*, 1456–1465.
97. Zhao, Y.; Truhlar, D.G. The M06 suite of density functionals for main group thermochemistry, thermochemical kinetics, noncovalent interactions, excited states, and transition elements: Two new functionals and systematic testing of four M06-class functionals and 12 other functionals. *Theor. Chem. Acc.* **2008**, *120*, 215–241.
98. Staroverov, V.N.; Scuseria, G.E.; Tao, J.M.; Perdew, J.P. Comparative assessment of a new nonempirical density functional: Molecules and hydrogen-bonded complexes. *J. Chem. Phys.* **2003**, *119*, 12129–12137.
99. Staroverov, V.N.; Scuseria, G.E.; Tao, J.M.; Perdew, J.P. Erratum: "Comparative assessment of a new nonempirical density functional: Molecules and hydrogen-bonded complexes [J. Chem. Phys. 119, 12129 (2003)]". *J. Chem. Phys.* **2004**, *121*, 11507.
100. Tao, J.M.; Perdew, J.P.; Staroverov, V.N.; Scuseria, G.E. Climbing the density functional ladder: Nonempirical meta-generalized gradient approximation designed for molecules and solids. *Phys. Rev. Lett.* **2003**, *91*, 146401–146404.
101. Adamo, C.; Barone, V. Toward reliable density functional methods without adjustable parameters: The pbe0 model. *J. Chem. Phys.* **1999**, *110*, 6158–6170.
102. Perdew, J.P.; Burke, K.; Ernzerhof, M. Generalized gradient approximation made simple. *Phys. Rev. Lett.* **1996**, *77*, 3865–3868.
103. Perdew, J.P.; Burke, K.; Ernzerhof, M. Erratum: Generalized gradient approximation made simple [phys. Rev. Lett. 77, 3865 (1996)]. *Phys. Rev. Lett.* **1997**, *78*, 1396–1396.
104. Miertus, S.; Scrocco, E.; Tomasi, J. Electrostatic interaction of a solute with a continuum—A direct utilization of abinitio molecular potentials for the prevision of solvent effects. *Chem. Phys.* **1981**, *55*, 117–129.
105. Barone, V.; Cossi, M.; Tomasi, J. Geometry optimization of molecular structures in solution by the polarizable continuum model. *J. Comput. Chem.* **1998**, *19*, 404–417.
106. Wiberg, K.B. Application of Pople-Santry-Segal CNDO method to cyclopropylcarbinyl and cyclobutyl cation and to bicyclobutane. *Tetrahedron* **1968**, *24*, 1083–1096.
107. Reed, A.E.; Weinstock, R.B.; Weinhold, F. Natural-population analysis. *J. Chem. Phys.* **1985**, *83*, 735–746.
108. Reed, A.E.; Curtiss, L.A.; Weinhold, F. Intermolecular interactions from a natural bond orbital, donor-acceptor viewpoint. *Chem. Rev.* **1988**, *88*, 899–926.
109. Glendening, E.D.; Badenhoop, J.K.; Reed, A.E.; Carpenter, J.E.; Bohmann, J.A.; Morales, C.M.; Weinhold, F. *Gennbo 5.9*; Theoretical Chemistry Institute, University of Wisconsin: Madison, WI, USA, 2009.
110. Wolters, L.P.; Bickelhaupt, F.M. The activation strain model and molecular orbital theory. *Wiley Interdiscip. Rev.-Comput. Mol. Sci.* **2015**, *5*, 324–343.
111. Bickelhaupt, F.M.; Houk, K.N. Analyzing reaction rates with the distortion/interaction-activation strain model. *Angew. Chem. Int. Ed.* **2017**, *56*, 10070–10086.
112. Morokuma, K. Moluecular orbital studies of hydrogen bonds 3. C=O H–O hydrogen bond in H_2CO and H_2O and H_2CO $2H_2O$. *J. Chem. Phys.* **1971**, *55*, 1236–1244.
113. Ziegler, T.; Rauk, A. Theoretical-study of the ethylene-metal bond in complexes between Cu^+, Ag^+, Au^+, Pt^0, or Pt^{2+} and ethylene, based on the Hartree-Fock-slater transition-state method. *Inorg. Chem.* **1979**, *18*, 1558–1565.
114. Ziegler, T.; Rauk, A. CO, CS, N_2, PF_3, and $CNCH_3$ as sigma-donors and pi-acceptors—Theoretical-study by the Hartree-Fock-Slater transition-state method. *Inorg. Chem.* **1979**, *18*, 1755–1759.
115. Bickelhaupt, F.M.; Nibbering, N.M.M.; Van Wezenbeek, E.M.; Baerends, E.J. Central bond in the three CN.cntdot.dimers NC-CN, CN-CN and CN-NC: electron pair bonding and Pauli repulsion effects. *J. Phys. Chem.* **1992**, *96*, 4864–4873.
116. Bickelhaupt, F.M.; Baerends, E.J. Kohn-Sham density functional theory: Predicting and understanding chemistry. In *Reviews in Computational Chemistry*; Lipkowitz, K.B., Boyd, D.B., Eds.; John Wiley & Sons, Inc.: Hoboken, NJ, USA, 2000; Volume 15, pp. 1–86.
117. Te Velde, G.; Bickelhaupt, F.M.; Baerends, E.J.; Fonseca Guerra, C.; van Gisbergen, S.J.A.; Snijders, J.G.; Ziegler, T. Chemistry with ADF. *J. Comput. Chem.* **2001**, *22*, 931–967.
118. Fernández, I.; Bickelhaupt, F.M. Deeper insight into the diels-alder reaction through the activation strain model. *Chem. Asian J.* **2016**, *11*, 3297–3304.
119. Fernández, I.; Bickelhaupt, F.M. The activation strain model and molecular orbital theory: Understanding and designing chemical reactions. *Chem. Soc. Rev.* **2014**, *43*, 4953–4967.

120. Krijn, J.; Baerends, E.J. *Fit Functions in the HFS-Method*; Internal Report (in Dutch); Free University: Amsterdam, The Netherlands, 1981.
121. Van Lenthe, E.; Baerends, E.J.; Snijders, J.G. Relativistic regular two-component Hamiltonians. *J. Chem. Phys.* **1993**, *99*, 4597–4610.